Journal of ELECTRICAL ENGINEERING, VOL 73(2022), NO4, 237–247

sciendo

PAPERS

Active-clamped flyback DC-DC converter in an 800V application: Design notes and control aspects

Darko Vračar[1,2], **Predrag Pejović**[1]

This paper presents findings for active-clamped flyback (ACF) DC-DC converter 57 W used as an auxiliary power-supply of a wireless inductive-charging system 800 V. Measurements of magnetizing and leakage inductances for three transformers demonstrated how big differences between them could be depending on chosen vendor. Comparison of simulated and measured Bode plots showed that, even when those plots were not matched, one could design a compensator that ensures stable operation. Evaluation of cross-regulation when output with low power (9.62 % of total) was regulated showed that such approach was feasible too. The *switching frequency vs output-power* and *drain-source voltage of switch vs output-power* graphs are presented for the first time. Comparison of bandwidth, phase-margin and gain-margin *vs*input-power, between the ACF and conventional flyback converter were discussed too. Those quantities were changeable with load and input-voltage as expected. The conventional flyback converter in DCM has higher bandwidth than the ACF which resulted in lower phase- and gain-margins. That showed that it cannot have the same compensator as an ACF.

K e y w o r d s: active-clamped flyback, Bode plots, control, cross-regulation, DC-DC converter, inductance measurement, switching-frequency change, transformer

1 Introduction

The active-clamped flyback (ACF) DC-DC converter is known for around 30 years [1]. Its mainstream application nowadays is as power adapter and sometimes with GaN transistors [2,3]. Typically, the ACF is supplied from the rectified single-phase mains [4,5]. Its general analysis, operation, and design are well explained in[6-9] so readers shall check those references for more information.

The first reported ACF application in a system with higher-DC-input-voltage (HDCIV) of 800 V was [4] followed by [5]. In those papers the 57 W ACF was used as an auxiliary power-supply (APS) of primary (*ie* ground) side of an inductive-charging system (ICS) for wireless-charging of battery electric-vehicles (BEV). The same application and converter is subject of this article with difference that transformer 400 μH and accordingly adapted electrical schematic were used. The APS powers system parts like gate-drivers, microcontroller, communication, voltage- and current-measurement circuitry, fan, ancillary circuitries, *etc*.

Motivation to writing this paper was to present missing theoretical considerations, simulation, and experimental results for the ACF that were not covered in [4] and [5]. Focus here is on transformer measurements, cross-regulation and control aspects with comparison to conventional flyback DC-DC converter. This article is a companion to [4] and [5]. Note that this article does not introduce a new topology or a control method but evaluates usage of the known topology (ACF) in an emerging application (ICS). However, the conclusions are applicable for any ACF. Moreover, since this study was part of a commercial project it was not possible to reveal all technical details — only minimum was presented that supported our conclusions.

The APS was connected to the 800 V variable DC-link as shown in Fig. 1, which is typical for industrial applications. The generic schematic of an ACF is presented in Fig. 2.

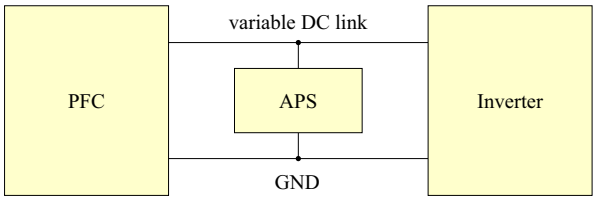

Fig. 1. The APS connection-point in the ICS

An ACF is different from conventional flyback converter in a sense that a bidirectional switch (QH) is introduced instead of the clamping diode in a passive RCD (resistor-capacitor-diode) snubber [4, 5]. The QH is actively controlled to increase ACF efficiency by storing energy in the clamping-capacitor C_C) then releasing it to the secondary side [4]. In this application one had to use external inductor to realize zero-voltage switching (ZVS) operation of the low-side switch (QL), [4]. The SW denotes switching node which is equal to drain-source voltage of QL. Note that the resonant inductance L_r), depicted in Fig. 2, comprises an external inductor and the

[1] School of Electrical Engineering, University of Belgrade, 11000 Belgrade, Serbia, [2] BRUSA Elektronik (München) GmbH, 81829 Munich, Germany, darko.vracar@brusa.biz

https://doi.org/10.2478/jee-2022-0032, Print (till 2015) ISSN 1335-3632, On-line ISSN 1339-309X

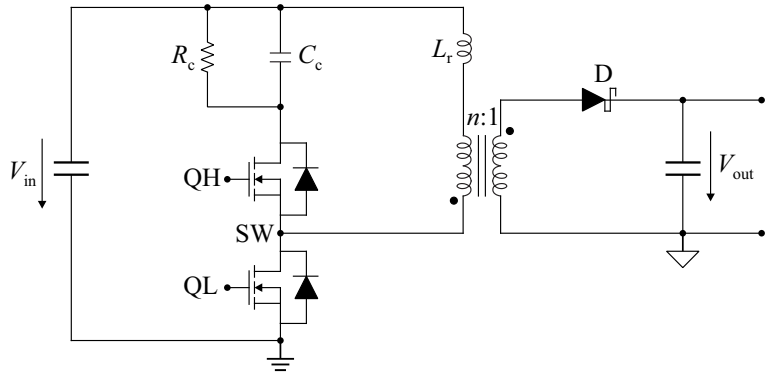

Fig. 2. The ACF generic schematics with resonant inductance

Table 1. The 57 W ACF specification

Parameter	Value
Input dc voltage (ICS power transfer)	620–880 V
Input dc voltage (ICS stand-by)	460–640 V
Output 1: regulated voltage	+5.5 V
Output 1: load current	1 A
Output 2: voltage	+5.5 V
Output 2: load current	2.15 A
Output 3: voltage	+22 V
Output 3: load current	1.7 A
Output 4/5: voltage	±11 V
Output 4/5: load current	±40 mA
Output power in stand-by mode	< 10 W
Minimum switching frequency, $f_{\mathrm{sw\,min}}$	66 kHz

leakage inductance. The general advantages and disadvantages of ACF versus conventional flyback converter were elaborated in [10], [5] as well as challenges when used in HDCIV applications, [5].

During literature review many gaps were identified. Majority was covered in [5] and rest will be covered here. The key-contributions are listed below.

- Comparison of magnetizing inductance *vs* primary current $L_{\mathrm{m}}(I)$ characteristics for three vendors with the same 400 μH transformer-specification. In addition, a change of leakage inductance *vs* current for those transformers was presented too. There one could see how big differences between vendors could be and design engineer shall take that into account.
- The efficiency graphs presented and compared for ACF with three 400 μH transformers. The efficiencies are lower at higher input voltages, as expected, due to higher circulation-energy losses [5].
- The *switching-frequency vs output-power* and *drain-source voltage QL vs output-power* graphs are presented for the first time for an ACF in an 800 V system. Both quantities were slightly changeable with load as expected.
- Comparison of simulated and measured Bode plots of ACF at 620 V and 850 V inputs was shown for the first time. It was demonstrated that, although those plots were not matched, one could still design a compensator that ensures stable operation over whole input voltage and load ranges.
- The cross-regulation of the ACF with five outputs was investigated in a case where regulated output was the one with only 9.62 % of the total power. This was contrary to the common approach in industry of regulating the output with the highest power. However, our results showed that this was feasible too.
- The method for measurement of opto-coupler's capacitance [11] is improved a bit in a sense that such capacitance is calculated as an average of two measurements at different operating points thus improving accuracy and plausibility of the result.
- Comparison of bandwidth, phase-margin, gain-margin vs. input power for an ACF and conventional flyback converters is presented for the first time. Both converters exhibited a first-order response that is typical for any peak-current controlled flyback DC-DC converter [12].
- For multi-mode control IC [13] in our case it was discovered that output power has to be $\geq$ 10 W so that the ACF can surely switch into active-clamping mode (ACM) of operation. With lower loads it operated in DCM (discontinuous-conduction mode) as conventional flyback converter or in transition between the two. This effect was probably inherent to how NCP1568 operates. One reason could be that this IC was not intended for use in the HDCIV applications.

2 Design notes

The specification of the 57 W ACF is given in Tab. 1, [4, 5]. The ACF has two operating ranges: ICS power-transfer mode and ICS stand-by mode. The used control IC was Onsemi NCP1568 multi-mode controller [13] with generic design-notes provided in [14].

Here transformer design notes and its measurements will be elaborated. More on ACF design, related challenges, and operation in ICS stand-by mode one can find in [5]. The resistor R_{C} in this study was 4.5 MΩ, *ie* the

Table 2. Specification of the transformer

Parameter	Value
Maximum primary working voltage	> 960 V
Clearance and creepage distances	> 7.9 mm
Turns ratio primary to output 1 & 2	15
Turns ratio primary to output 3	3.75
Turns ratio primary to output 4 & 5	7.5
Core shape	ETD29
Core material	N87, TP4, DMR40
Magnetizing inductance, L_m	$400\,\mu$H
Max peak primary-current, $I_{\mathrm{pri\,max}}$	2.32 A

Table 3. Overview of the used transformers

Type: L_m (μH)	vendor	n_eff
T2-1: 400,	2	14.43
T2-2: 400,	3	15.74
T2-3: 400,	1	15.76–15.81
T3-1: 600,	1	15.53–15.54
T3-2: 600,	2	13.65
T3-3: 600,	3, rev.1	14.81–14.93
T3-4: 600,	3, rev.2	14.96–15.03

hybrid-clamp [5] was not used – but that had no influence to the results.

Note that with NCP1568 the ACF can operate in DCM like conventional flyback DC-DC converter and in ACM. The ACM can be with magnetizing current going into negative direction (called DCM ACM) or being positive all the time. The latter case is called CCM (continuous-conduction mode) ACM. Our case is the DCM ACM and both terms ACM and DCM ACM will be used in paper interchangeably.

2.1 Transformer design

The design of an ACF transformer is like any other flyback one. Hence, only few notes will be given here. A comprehensive study on transformer design for DCM flyback with multiple outputs is presented in [15]. In [16] is claimed that biggest portion of losses in DCM flyback comes from transformer itself. The key-data of the transformer 60 W, that was used, are listed in Tab. 2 with schematic symbol shown in Fig. 3. It was slightly overdesigned than the required power of 57 W to have some reserve if project requirements change later. The auxiliary winding (Fig. 3) provides self-supply for the control IC and half-bridge driver of QL and QH.

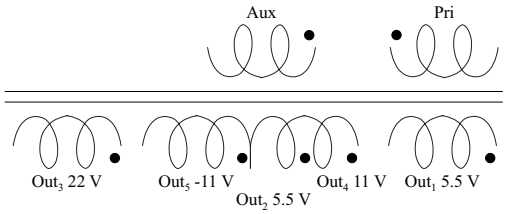

Fig. 3. The schematic symbol of the transformer T2

The ETD29 bobbin had to be used in order to house two primary and five secondary windings, and to satisfy requirements for clearance and creepage safety-distances ($>$ 7.9mm), [5]. The safety-distances were calculated per [17]. In our case, going for a switching-frequency higher than 70 kHz would not bring advantage in potential transformer-size reduction [4], but would only increase converter losses. In addition, the transformer leakage-inductance ($\leq 9\mu$H) was not enough for the ZVS operation. Hence, an external inductor of 68μH had to be used to ensure ZVS of the QL.

The magnetizing inductance in Tab. 2 is chosen as [5]

$$L_m < 0.95\,\min(L_\mathrm{msb}, L_\mathrm{mpt}), \tag{1}$$

where L_msb and L_mpt are magnetizing inductances for ICS stand-by (sb) and power-transfer (pt) modes, respectively, with tolerance-correction factor of 0.95 [5]. Respective inductances are calculated per [5]

$$L_\mathrm{m} = \frac{D_\mathrm{max}^2 V_\mathrm{in\,min}^2 \eta}{2 P_\mathrm{out} f_\mathrm{sw\,min}}, \tag{2}$$

where D_max is maximum duty-cycle (16 % or 12 %), $V_\mathrm{in\,min}$ is minimum input DC voltage, η – is assumed maximum efficiency (70 % or 85 %), P_out total output-power (10 W or 57 W), [5].

The values for L_msb and L_mpt were 3.44 mH and 0.66 mH, respectively, [5]. Hence, the L_m was chosen to be 400 μH. Such transformer would allow minimum switching frequency of 100 kHz, but that was not used here due to increased losses.

2.2 Transformer measurements

The transformers were designed and built by three companies per specification in Tab. 2. They were potted and belong to temperature-class B (130 °C). A representative photo is shown in Fig. 4. Full details of their construction and design process are not known to us. We assume that basic differences are coming from different wires and air-gap used. A major challenge when working with custom-designed magnetic parts is that delivery times could be very long (*eg* 7–11 weeks), [5].

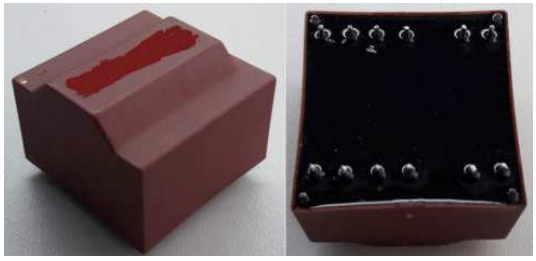

Fig. 4. Photo of the transformer T2-3

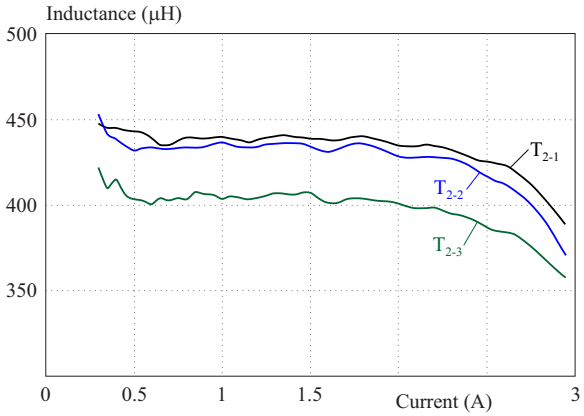

Fig. 5. The magnetizing-inductance *vs* primary current characteristics of transformers 60 W, ETD29 measured at room temperature

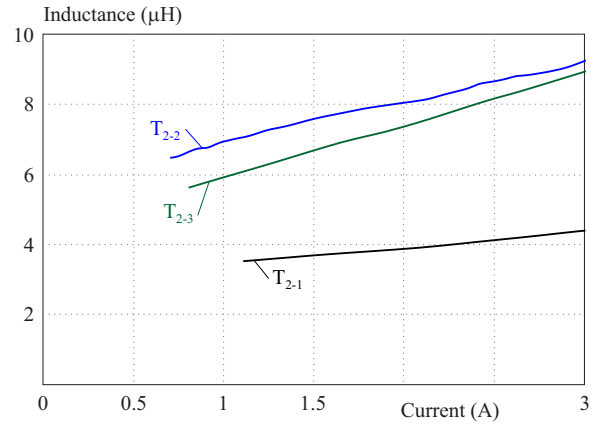

Fig. 6. The leakage-inductance change of transformers ETD29 measured at room temperature

In Tab. 3 a summary of the used transformers is presented together with effective turns-ratio n_{eff}. The leakage inductances for all of them were $\leq 9\,\mu$H. Note that transformers 600 μH are included in Tab. 3 although they are not subject of simulation and experimental results here. This is done to complement info in Table V provided in [5]. The transformer markings in Tab. 3 is like the style used in [5]. Note that the T2-1 in [4] was named as T2.

The calculated turns-ratio (primary to the regulated +5.5 V output) was 15 (Tab. 2). However, in Tab. 3 one can see that effective turns-ratio (3) varies between vendors in range $-3.8\,\%$ to $+5.4\,\%$ (400 μH) and in range $-9\,\%$ to $+3.6\,\%$ (600 μH) versus the rated one. It was calculated as

$$\eta_{\text{eff}} = \sqrt{\frac{L_{m,\,\text{me}}}{L_{\text{out1,\,me}}}}, \tag{3}$$

where $L_{\text{m, me}}$ is the measured magnetizing-inductance and the is $L_{\text{out1, me}}$ is the measured inductance of output 1. Those values were measured with a precision LCR-meter.

When evaluating efficiencies in [4] and [5] it was noticed that highest ones were for designs with vendor 2 (T2-1 and T3-2). This suggested that either constructions by vendor 2 had lower AC, DC and core losses and/or that optimal turns-ratio is below 15. This will be analyzed in a separate study.

The characteristic $L_{\text{m}}(I)$, measured by Power Choke Tester [18], are presented in Fig. 5. From it one can understand how transformer characteristic could be different for different vendors although the same specification was given. The $L_{\text{m}}(I)$ characteristic is good to have to see when the saturation sets-in and how slope looks like. That is what the ACF faces in real operation.

From Fig. 5 can be seen that during operation at 66 kHz peak current would be 2.32 A which corresponds to 428 μH (T2-1). One can assume, that at higher temperatures, the magnetizing inductance would be lower and at knee of the characteristics (around 400 μH for T2-1), *ie* at beginning of the saturation. Such a design ensures good utilization of the magnetic material, hence reduces costs.

The measured leakage inductances of transformers are shown in Fig. 6. All secondary windings and auxiliary winding were shorted together during those measurements. One can notice that leakage inductances vary linearly with the primary current as expected. Moreover, we see how values are different for different vendors. At lower currents the test device does not displays the measured inductance probably due to high measurement-error which was not needed anyway. As elaborated in [10], if precision LCR-meter would have been used to measure leakage inductance one would wrongly conclude that it is constant – which is not the case. For example, for the T2-3 the 6 μH was measured.

For some cases in mainstream applications, if primary leakage inductance is big enough, it was suggested that one does not have to use external inductor [14]. However, for HDCIV applications that was impossible to avoid [4, 5, 10]. In addition, in ICS application one has several secondary outputs hence relationship between leakage inductances became more complex and that may influence the cross-regulation behavior of the ACF [19, 20].

3 Simulation results

The 57 W ACF with 400 μH transformer was simulated in SIMPLIS [21]. More info about used simulation models of NCP1568 one can find in [4, 10]. Typical simulation run-time for 50.2 ms was 11—12 s. The total parasitic capacitance of the switching node C_{SW} was estimated to be $\approx$ 186 pF, [5]. During experiments, the switching-frequency was slightly varying with the load and input voltage ($\approx$ 66–68 kHz, see Fig. 15) therefore simulations were executed at 67 kHz. The external inductor (L_{e}) and clamping capacitor C_{C} had values of 68 μH and 66 nF, respectively. Sometimes they are named as resonant-tank parameters and have influence on the converter efficiency [4, 5]. Focus in this section will be on ICS power-transfer mode (ACF in ACM) since, in the

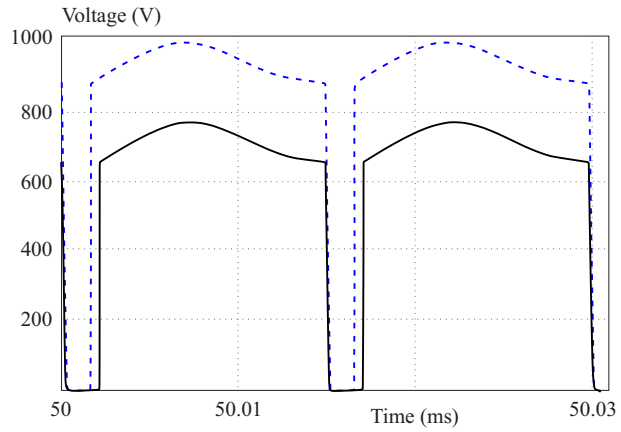

Fig. 7. The ACF 57 W drain-source voltages in steady-state at 620 V (black solid line) and 850 V (blue dashed line) inputs and rated load in ACM

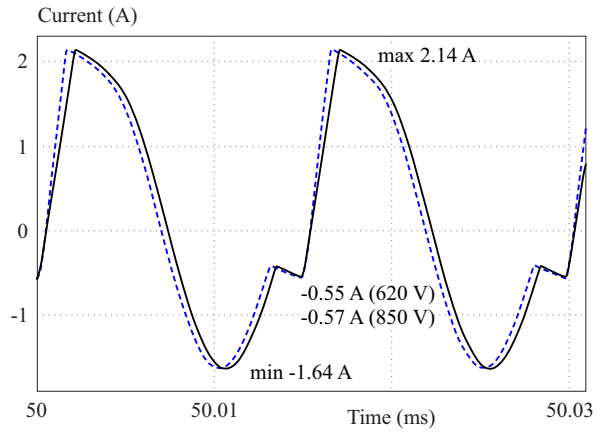

Fig. 8. The simulated primary currents at 620 V (black solid line) and 850 V (blue dashed line) at rated load in ACM.

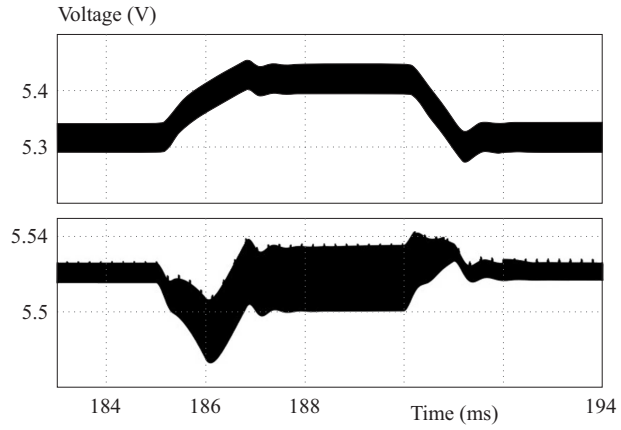

Fig. 9. The dynamic load-change at 620 V input in ACM. Upper trace: non-regulated 5.5 V output with 2.2 A load. Bottom trace: regulated 5.5 V output with load change from 0.2 A to 1 A and vice versa

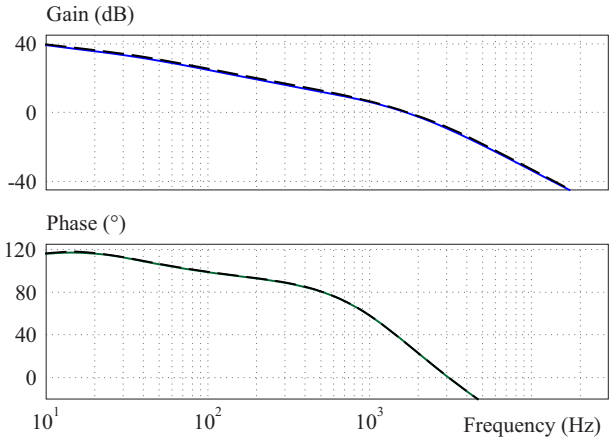

Fig. 10. The simulated Bode plots at 620 V (solid lines) and 850 V (black dashed lines) inputs at rated load in ACM

ICS stand-by mode, the ACF behaves like conventional flyback converter in DCM (*ie* disabled-ACM) [5].

3.1 Operation in ICS power- transfer mode

Detailed simulation results and comparisons of ACF with 400 μH and 600 μH transformers were provided in [4]. Only few waveforms are repeated here (Figs. 7 and 8), but in a different way for the sake of paper completeness. The simulation results of QL drain-source voltages V_{DS} at 620 V and 850 V DC inputs and 57 W are shown in Fig. 7. There one can notice that the active-clamping is working as expected and that duty-cycles are different (13.32 % *vs* 9.22 %). The maximum voltages of QL (*ie* SW node) were ≈ 773 V (at 620 V) and ≈ 1002 V (at 850 V).

Primary currents are presented in Fig. 8. In our ACF, the magnetizing current (hence primary current) must go into negative direction to discharge the parasitic capacitance of the switching node thus ensuring ZVS of the QL. This is achieved as can be seen in the Fig. 8 as well as that the resonant period is finished before QH is turned-off.

3.2 Dynamic load-change

The simulation of dynamic load-change at +5.5 V regulated output with 620 V input is shown in Fig. 9. There it can be noticed that regulator works as expected with minimum deviations of regulated (5.473–5.543 V) and non-regulated (5.274–5.454 V) +5.5 V outputs. In addition, one can see at the regulated output that ripple is higher at higher load as expected. Note that the non-regulated output has lower value than rated one because that depends on load at the regulated output (*ie* with 0.2 A there is not enough gain). The other outputs had rated loads. The results for 850 V are not included since they are better than the 620 V ones.

3.3 Bode plots at 620 V and 850 V

With SIMPLIS it was very easy and fast (5–7 s) to generate the Bode plots. The adjusted settings of parametrized opto-coupler in SIMPLIS were: current transfer-ratio 1.6, 1-st pole frequency 4 kHz and output capacitance of 3.07 nF.

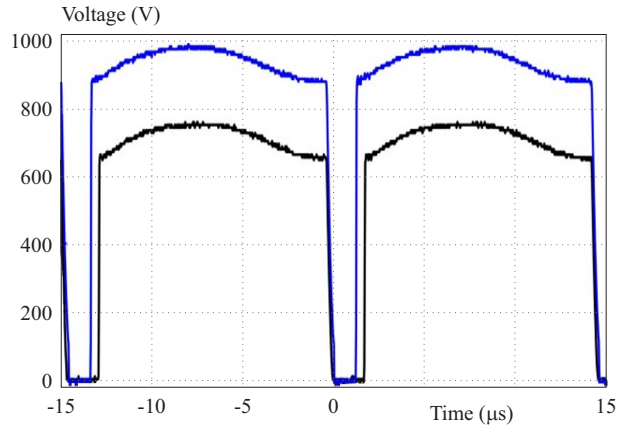

Fig. 11. The 57 W ACF (T2-1) operating at 620 V (black line) and 850 V (blue line) inputs and rated load in ACM

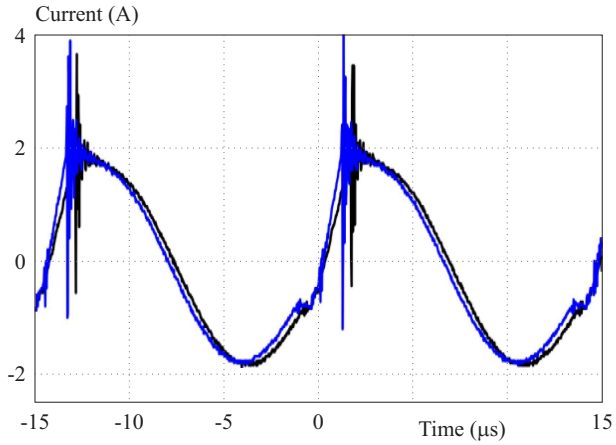

Fig. 12. The 57 W ACF (T2-1) operating at 620 V (black line) and 850 V (blue line) inputs and rated load in ACM

In Fig. 10 simulated Bode plots at 620 V and 850 V are shown. Both simulation runs were executed at rated load in DCM ACM with 400 μH transformer and 68 + 9 μH resonant inductance. The Fig. 10 shows that there is no significant difference between simulated Bode plots in operation at 620 V and 850 V. Whether in reality is like that we will find out in the experimental section where detailed findings are summarized in Tab. 4. Furthermore, in Fig. 10 one can notice first-order response – which is expected for any peak-current controlled flyback DC-DC converter [12].

4 Experimental results and discussion

The ACF, as specified in Tab. 1, was built and tested. Detailed photo of the 57 W ACF on a demo-board is provided in [4] whereas photo of system implementation is presented in [5]. The PWB (printed-wiring board) was done as a 4-layer one with FR-4 material and 70 μm copper on outer layers.

Tests were executed in a way that both 5.5 V and 22 V outputs were loaded by DC-electronic-loads and the ±11 V outputs had only bleeder resistors of 10 kΩ as loads [5]. This was done to make testing easier and had no influence on the findings [5]. The DC-supply-voltage was provided by a high-voltage DC-source.

4.1 Operational waveforms in ICS power-transfer mode

The key waveforms are presented in Figs. 11 and 12. Those results are repeated from [4], but in a different way for the sake of paper completeness and easier comparison with Figs. 7 and 8. Note that the saved oscilloscope dataset was used for the figures plotting. Hence, the negative-time is a consequence of the oscilloscope trigger at zero instant.

In Fig. 11 we see QL drain-source voltages at 620 V and 850 V input and rated load in ACM. Maximum values were 761 V and 994 V, respectively. Additionally, one can see that the maximum drain-source voltages are little bit lower than in simulations (Fig. 7). The differences are ≈ 12 V at 620 V and ≈ 8 V at 850 V. That is good for the design because it is on a side of safety.

The maximum and minimum currents on primary side (Fig. 12) are a bit higher than the simulated ones. The minimum values were −1.89 A (620 V) and −1.85 A (850 V). For positive values it was hard to estimate exact values due to ringing. Although layout was done carefully the ringing of primary current during dead-time, within commutation process between QL and free-wheeling diode of QH, was unavoidable (Fig. 12). In this period one actually has resonant tank comprising the C_{SW}, clamping capacitor, magnetizing and resonant inductance.

For negative values the absolute differences were 245 mA (+14.9 %) at 620 V and 208 mA (+12.7 %) at 850 V but are acceptable. In addition, we see that resonant periods are a bit longer than in simulations (Fig. 8) — which is a consequence of component tolerances.

The switching-frequency *vs* load curve is shown in Fig. 13 for the first time for an ACF in 800 V applications. The NCP1568 uses external resistor on pin 5 (RT) to ground which sets the minimum frequency of the internal oscillator [13]. This means that the switching frequency cannot go below the minimum set value. In our case that was around 63–64 kHz ($R(RT)$ = 160 kΩ). It was noticed that, at different loads and input voltages, the switching frequency was not changing significantly — contrary to what was often reported in literature. It is worth noting that such curves with 13 W ACF (Fig. 17 in [10]) have similar trends, *ie* those results are plausible for the HDCIV applications.

In Fig. 14 the change of maximum QL drain-source voltage with load is presented for the first time. One can clearly see that this value is not constant and that is rises with increasing load — which makes sense due to higher energy in leakage inductance. Hence the designer shall take that into account during development. The voltage increase was 24 V (+3.2 %) at 620 V and 32 V (+3.3 %) at 850 V. Note that results shown in Figs. 13 and 14 are

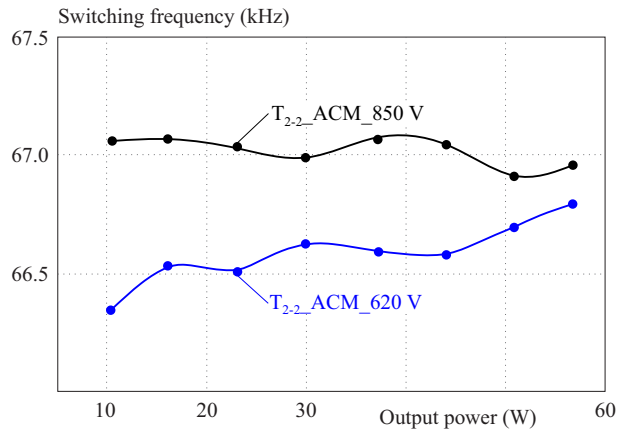

Fig. 13. The 57 W ACF (T2-2) measured switching frequency *vs* load curves in ACM

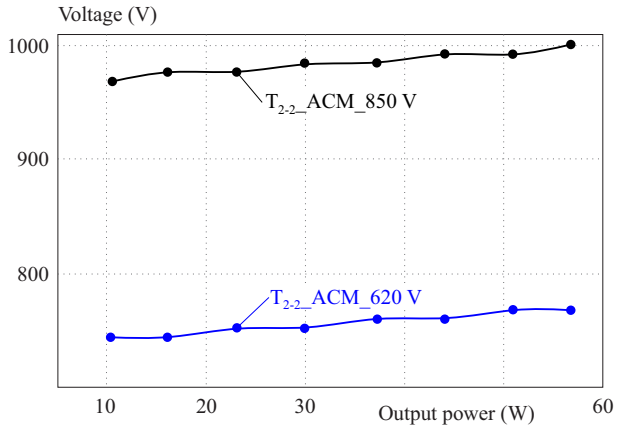

Fig. 14. The 57 W ACF (T2-2) measured maximum QL drain-source voltage *vs* load curves in ACM

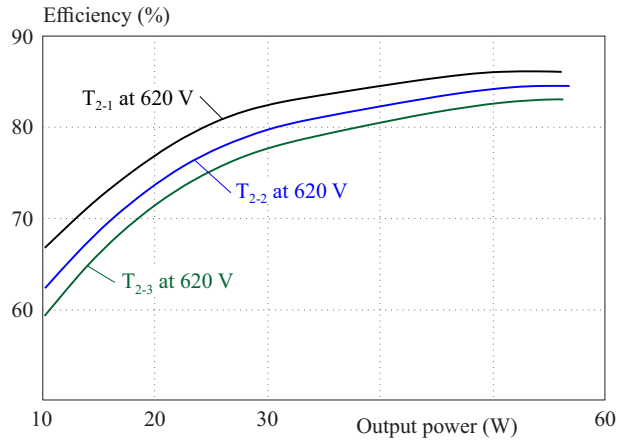

Fig. 15. The 57 W ACF efficiency curves with 620 V input in ACM

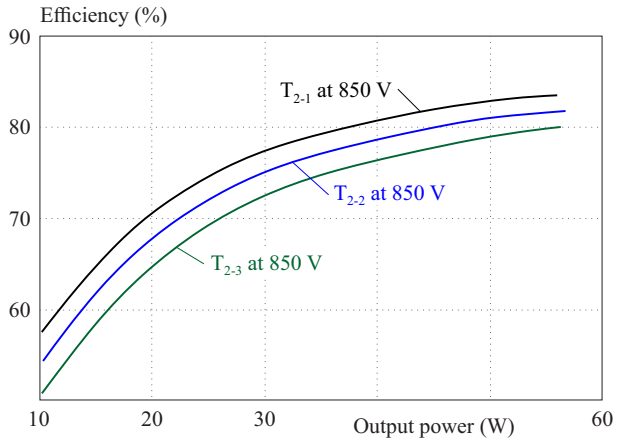

Fig. 16. The 57 W ACF efficiency curves with 850 V input in ACM

read from the oscilloscope screen and might be prone to the measurement errors.

The NCP1568 can operate in forced ACM (*ie* no multi-mode) by choice of two external resistors [13]. However, during tests it was noticed that around 10 W total load is needed for ACF to switch into ACM operation. That is the reason why all experimental results in Section 4 have results with loads $\geq$ 10 W. Anyway, for ICS that was not a problem since minimum typical load $\geq$ 15 W so one has enough reserve. At loads lower than 10 W the ACF was operating in DCM as conventional flyback converter or in kind of a transition between DCM and ACM. This effect is probably inherent to how NCP1568 operates, but might be further investigated in a separate study. One of the reasons could be that this IC was not intended for use in HDCIV applications.

4.2 Efficiency measurements

The efficiency measurements are provided in Figs. 15 and 16 for T2 transformers. The self-consumption of the primary side was considered. Those graphs clearly show how different transformer constructions (mainly choice of wires for windings and air-gap) are influencing the converter efficiency. Interesting is to notice that all curves are almost parallel (*ie* shifted) to each other. As expected, the efficiency at lower input voltage is higher due to lower losses in the resonant tank [5, 10].

More on the circulation-energy losses one can find in [5]. Maximum efficiencies of 86.1 % at 620 V and 83.5 % at 850 V inputs were achieved with T2-1 and $\approx$ 55.8 W load. The efficiency-measurements in [4, 5, 10] show the similar trends and curve-shapes — which guarantees plausibility of our measurements.

4.3 Control aspects

In this section we will present results that complement the ones presented in [5]. Important to know is that the ACF in DCM ACM is a combination of a PWM converter (during on-time) and a resonant one (during off-time) [5, 22, 23]. That feature complicated its small-signal analysis in the past [5], but it is solved now [22–25]. The key-paper for understanding of the NCP1568 operation with three control-loops (voltage, current and switching-period) is [24].

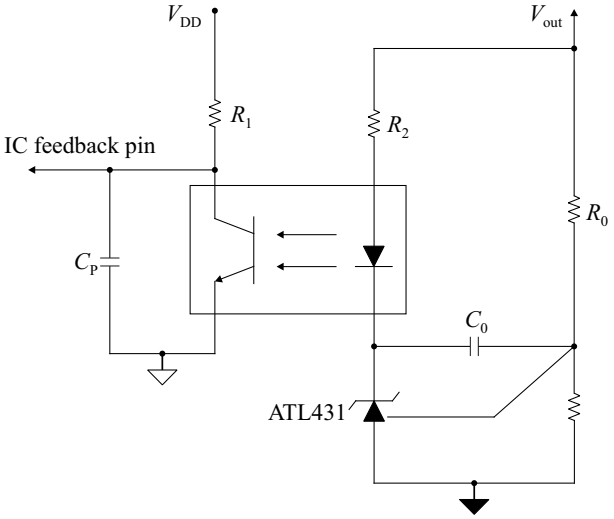

Fig. 17. The generic Type-2 compensator with shunt regulator and opto-coupler

The compensator used was the ATL431 [26] based Type-2 one (integrator, one pole and one zero) with an opto-coupler [5]. Its generic form is shown in Fig. 17 and transfer function in (4)–(6). Due to commercial nature of this project the values of components are not revealed. The compensator key-parameters were dc-gain of 34.1 dB, zero at 8.8 Hz, and pole at 4.97 kHz, [5]. The used opto-coupler had minimum current-gain (CTR) of 1.6 and its parasitic capacitance of 3.07 nF was estimated per method in [11]. Here, that method is improved a bit in a sense that opto-coupler's capacitance is calculated as an average of two measurements at different operating points thus improving accuracy and plausibility of the result. Those measurements were executed with different values of injection resistors (1 kΩ and 13 kΩ) hence currents through opto-coupler's diode were 1.7 mA and 0.4 mA, respectively. In both cases the V_{CC} was 5 V.

The transfer function of compensator from Fig. 18 is

$$G(s) = -G_0 \frac{1 + \dfrac{\omega_z}{s}}{1 + \dfrac{s}{\omega_p}}, \tag{4}$$

where G_0 is DC gain, ω_z, ω_p are the zero and the pole angular frequency. The DC gain is calculated as

$$G_0 = C_T \frac{R_1}{R_2}, \tag{5}$$

whereas zero and pole frequencies are calculated as

$$\omega_z = \frac{1}{R_0 C_0}, \quad \omega_p = \frac{1}{R_1 C_P}. \tag{6}$$

Note that C_P represents parallel connection of external capacitor (if any) and opto-coupler's (parasitic) capacitance.

4.3.1 Bode plots in ACM

The Bode plots of 57 W ACF operating in DCM ACM, with T2-2 transformer, were measured with Bode 100 vector network-analyzer [27]. Excitation signal was 20–30 mV (peak-to-peak). Measurements of Bode plots at 620 V and 850 V, with rated load, are shown in Figs. 18 and 19, respectively. The both measured plots show a first-order response that is typical for any peak-current controlled flyback DC-DC converter [12]. Additionally, respective simulation results are included in Figs. 18 and 19 for better comparison.

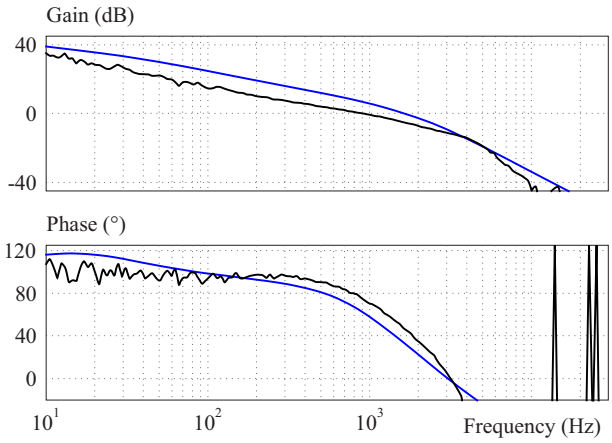

Fig. 18. The simulated (blue lines) and measured (black lines) Bode plots at 620 V and rated load in ACM

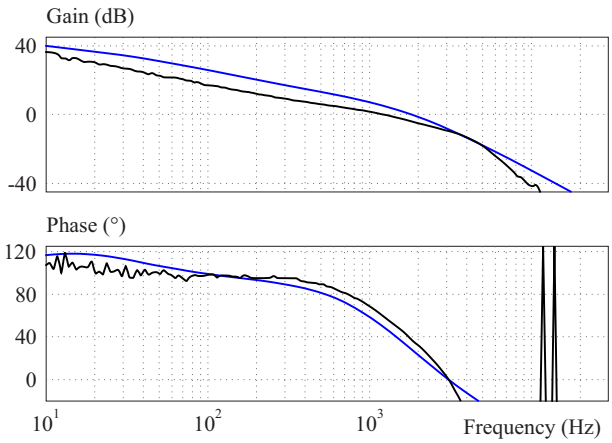

Fig. 19. The simulated (blue lines) and measured (black lines) Bode plots at 850 V and rated load in ACM

The overview of simulated and measured data from Bode plots at rated load is given in Tab. 4 to ease comparison. Since PM and GM were enough high ($> 45°$, ≥ 10 dB) and the gain-characteristics were crossing zero-gain-point with slope of -20dB/decade we conclude that our ACF is stable from control-theory point of view. In Tab. 4 one can also see significant discrepancy between simulated and measured results for both input-voltages. However, the designed converter was stable in whole input-voltage and load ranges and that is what counts in practice. The simulated results helped only to notice

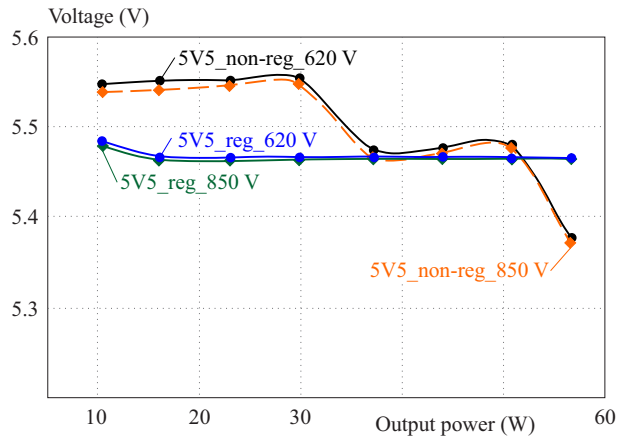

Fig. 20. The regulated 5.5 V (solid lines) and non-regulated (dashed lines) outputs for ACF in ACM at 620 V (black) and at 850 V (red)

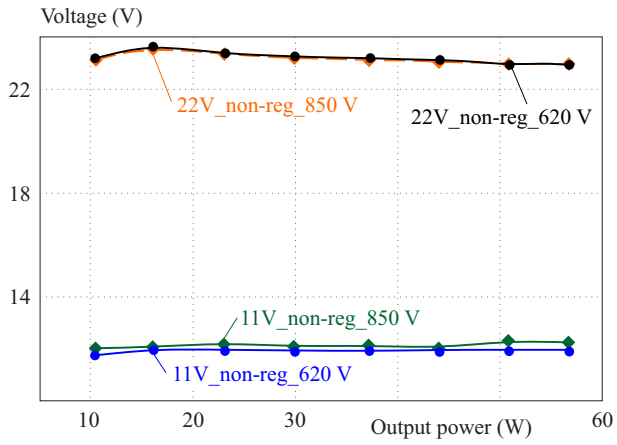

Fig. 21. The non-regulated 11 V (solid lines) and non-regulated 22 V (dashed lines) outputs for ACF at 620 V (black) and at 850 V (red)

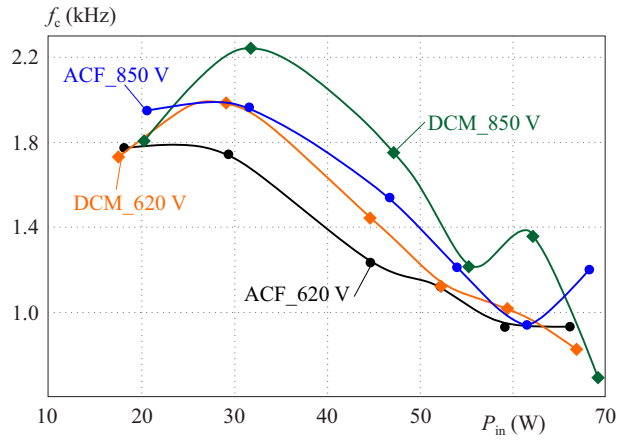

Fig. 22. The ACF in ACM vs. conventional flyback converter in DCM: bandwidth change with input voltage and input power

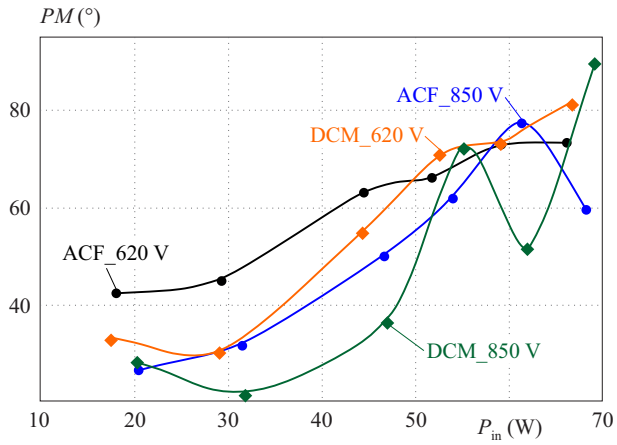

Fig. 23. The ACF in ACM vs. conventional flyback converter in DCM: phase-margin change with input voltage and input power

Table 4. Comparison of Bode plots at rated load

620 V	Simulated	Measured
Bandwidth, Hz	1718	938
Phase margin, deg	31.4	73.4
Gain margin, dB	9.3	11.5

850 V	Simulated	Measured
Bandwidth, Hz	1832	1211
Phase margin, deg	27.8	59.9
Gain margin, dB	8.4	9.6

trends of change — which was helpful during design-phase to fine-tune the compensator.

4.3.2 Cross-regulation

The analysis and mathematical modeling of cross-regulation effect with flyback converters is well covered in literature [19, 20]. Some practical engineering tips were given in [28]. This effect is unavoidable and depends on magnetizing inductance, leakage inductances of primary and secondary windings and clamp-voltage [20].

Here we will elaborate the cross-regulation behavior of our ACF with five outputs. In this design voltage fluctuations on non-regulated outputs at lighter load were under control by using bleeder resistors, Zener diodes and stacked windings [28].

The regulated output was the 5.5 V one which had 5.5 W (9.62 % of the total power). This was contrary to the common approach in practice of regulating the output with the highest power. That was the 22 V one in our case with 38.4 W (67.22 % of total power). The reasons for such an approach were different reference (*ie* ground) potentials and different loading of the outputs depending on the ICS operation modes.

In Figs. 20 and 21 the voltage changes are presented for T2-2. One can see that the regulated output behaves as expected and that voltage fluctuations of non-regulated outputs are acceptable. That depended also on sequence of the outputs' loading, but in our case that was chosen in accordance with expected behavior of the ICS. Those

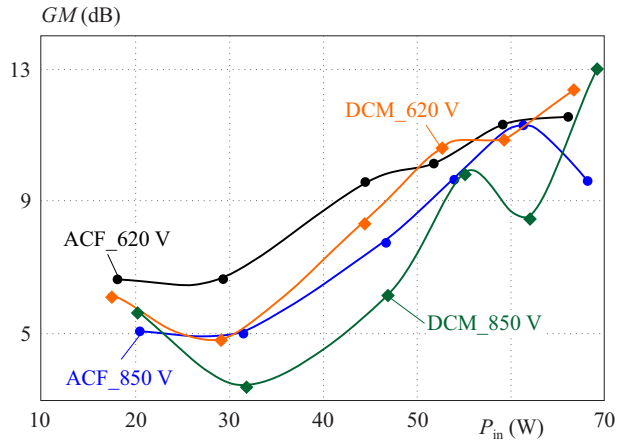

Fig. 24. The ACF in ACM *vs* conventional flyback converter in DCM: gain-margin change with input voltage and input power

results show that in normal operation no problems are expected.

4.3.3 Comparison to a conventional flyback converter

The ACF was modified into conventional DCM flyback DC-DC converter by disabling QH gate-signals, shorting inductor, and reducing resistors' values in the clamping circuit to 31 kΩ. Advantage of this method was that one had the same control IC, compensator, transformer (T2-2), and rest of the circuitry [5]. For ICS application, the conventional DCM flyback converter has higher efficiency at loads below 50 %, occupies 11 % less space and is 23 % cheaper [5]. The only advantage of an ACF in ICS might be reduced electro-magnetic interference (EMI) [5, 29].

Here we will present comparison of ACF Bode plots from [5] versus conventional flyback converter in DCM. The excitation signal was 35–40 mV (peak-to-peak). From Bode plots, for each measured point, the bandwidth, PM, and GM were extracted. The results are plotted in Fig. 22 to Fig. 24. Those quantities were plotted vs. input power because that was easier to do. Operation at six loads and two input voltages were measured. We see that conventional flyback converter in DCM has higher bandwidth than ACF which resulted in lower PM and GM. This suggests that the compensator needs adjustments to improve stability of conventional flyback converter in DCM. Bottom line: ACF in DCM ACM and conventional flyback in DCM with the same specification cannot share the same compensator.

5 Conclusion

In this paper, a 57 W ACF, supplied from an 800 V variable dc-link, was investigated. The ACF was used as an auxiliary power-supply of a wireless ICS for BEV. The simulation and experimental results of voltage waveforms were matched whereas current waveforms had acceptable deviations. Although simulated and measured Bode plots were not matched, the simulations were enough good to help design a good compensator — which was verified experimentally. As a result, the designed ACF was stable in whole load and input-voltage ranges.

Attention was paid to the transformer design and measurements of its magnetizing and leakage inductances vs. primary currents as well. Also, the *switching frequency vs load* curves were included as well as *maximum drain-source voltage of QL vs load* for the first time. This improved understanding of the ACF operation with variable switching-frequency. The regulation of output with 9.62 % of the total power — contrary to the common approach by regulating the biggest one — was proven to be feasible. As a last point, the f_C, PM, and GM changes were compared between ACF and conventional DCM flyback for the first time. It was showed that those converters, for the same specification, cannot share the same compensator.

Focus of the future work could be on mathematical modelling of Bode plots' differences between ACF and conventional flyback converter and mathematical analysis of the ACF cross-regulation effects.

Acknowledgements

This work was supported by BRUSA Elektronik (München) GmbH, Munich, Germany; www.brusa.biz. The support from its management and colleagues is highly appreciated as well. Authors also thank onsemi, United Silicon Carbide Inc. and transformer suppliers for support. The same free software was used as listed in the Acknowledgment section in [5].

References

[1] K. Yoshida, T. Ishii, and N. Nagagata, "Zero voltage switching approach for Flyback converter", *Proceedings of Fourteenth International Telecommunications Energy Conference – INTELEC '92*, Washington, DC, USA, pp. 324-329. 1992, doi: 10.1109/INTLEC.268424.

[2] X. Huang, J. Feng, W. Du, F. C. Lee, and Q. Li, "Design consideration of MHz active clamp Flyback converter with GaN devices for low power adapter application", *IEEE Applied Power Electronics Conference and Exposition (APEC)*, Long Beach, CA, USA, Mar 2016, pp. 2334–2341, doi: 10.1109/APEC.7468191.

[3] A. Zaman and A. Radić, "How to design and implement an adapter power supply with active clamp Flyback: An all silicon design methodology", *IEEE Power Electronics Magazine*, vol. 7, no. 4, pp. 36–43, Dec2020, doi:10.1109/MPEL.3033608.

[4] D. Vračar and M. Pavlovský, "Implementation of active-clamped Flyback DC-DC converter in an 800 V system", *PCIM Europe digital days*, pp. 1163–1170. 2021, https://ieeexplore.ieee.org/document/9472384.

[5] D. Vračar and P. Pejović, "Active-Clamp Flyback Converter as Auxiliary Power-Supply of an 800 V Inductive-Charging System for Electric Vehicles", *IEEE Access*, vol. 10, pp. 38254-38271, 2022, doi:10.1109/ACCESS.2022.3165059.

[6] R. Watson, F. C. Lee, and G. C. Hua, "Utilization of an active-clamp circuit to achieve soft switching in Flyback converters", *IEEE Trans. on Power Electronics*, vol. 11, no. 1, Art. no. 1, 1996, doi:10.1109/63.484429.

[7] B.-R. Lin, H.-K. Chiang, K.-C. Chen, and D. Wang, "Analysis, design and implementation of an active clamp Flyback converter", *International Conference on Power Electronics and Drives Systems*, Kuala Lumpur, Malaysia, vol. 1, pp. 424–429, 2005 doi:10.1109/PEDS.2005.1619724.

[8] J. Zhang, X. Huang, X. Wu, and Z. Qian, "A high efficiency Flyback converter with new active clamp technique", *IEEE Trans.on Power Electronics*, vol. 25, no. 7, July 2010, doi:10.1109/TPE L.2010.2042302.

[9] P.-H. Liu, "Design consideration of active clamp Flyback converter with highly nonlinear junction capacitance", *IEEE Applied Power Electronics Conference and Exposition (APEC)*, San Antonio, TX, USA, pp. 783-790, Mar 2018, doi:10.1109/APEC.2018.8341101.

[10] D. Vračar, M. Pavlovský, and P. Pejović, "Active-clamped Flyback DC-DC converter in three-phase application", *21st International Symposium on Power Electronics (Ee)*, Novi Sad, Serbia, pp. 1-6. Oct 2021, doi: 10.1109/Ee53374.2021.9628263.

[11] A. Shirsavar, *How to measure the Frequency of an Opto-Isolator for Power Supply Applications*, (Jan. 03, 2018), Aug 31, 2021 [*Online video*], https://www.youtube.com/watch?v=Eq8hGJ2ZLac.

[12] C. Basso, *Switch-Mode Power Supplies: Spice Simulations and Practical Designs*, 2nd ed. USA: McGraw-Hill Professional, 2014.

[13] Datasheet, "NCP1568: AC–DC active clamp Flyback PWM IC", Onsemi, 2021, [*Online*, https://www.onsemi.com/pdf/datasheet/ncp1568-d.pdf.

[14] White Paper, "High-density AC-DC power supplies using active-clamp Flyback topology", Onsemi, 2021, https://www.onsemi.com/pub/collateral/tnd6279-d.pdf.

[15] A. Ayachit, A. Reatti, and M. K. Kazimierczuk, "Magnetising inductance of multipleoutput flyback DC-DC convertor for discontinuousconduction mode", *IET Power Electronics*, vol. 10, no. 4, pp. 451–461, Mar 2017, doi: 10.1049/iet-pel.2016.0390.

[16] H. Onay, V. Suel, T. Ozgen, and A. Hava, "Comparative Power Loss Analysis of DCM Flyback Transformer Based on FEA, Numeric Simulation, Calculation and Measurements", *21st European Conference on Power Electronics and Applications* (EPE '19 ECCE Europe), Genova, Italy, pp. 1–10, doi: 10.23919/EPE.2019.8915387, 2019.

[17] IEC 61558-2-16:, "Safety of transformers, reactors, power supply units and combinations thereof – Part 2-16: Particular requirements and tests for switch mode power supply units and transformers for switch mode power supply units for general applications", IEC, https://webstore.iec.ch/ publication/65385, 2021.

[18] Description and technical specifications, "Power choke tester DPG10B series", ED-K, www.ed-k.de, 2021.

[19] D. Maksimović and R. Erickson, "Modeling of cross-regulation in multiple-output flyback converters", *APEC '99. Fourteenth Annual Applied Power Electronics Conference and Exposition. Conference Proceedings* (Cat. No.99CH36285), Dallas, TX, USA, vol. 2, pp. 1066–1072, 1999, doi: 10.1109/APEC.1999.750501.

[20] C. Ji, M. Smith, K. M. Smedley, and K. King, "Cross regulation in flyback converters: analytic model and solution", *IEEE Trans. Power Electron*, vol. 16, no. 2, pp. 231–239, 2001, doi: 10.1109/63.911147.

[21] Software (commercial), *SIMetrix/SIMPLIS ver. 8.50g Advanced Power System Simulation*, USA: Simplis Technologies Inc, 2021.

[22] S. Xu, Q. Qian, B. Ren, and Q. Liu, "An Accurate Small Signal Modeling and Control Loop Design of Active Clamp Flyback Converter", *10th International Conference on Power Electronics and ECCE Asia* (ICPE - ECCE Asia), Busan, Korea (South), pp. 3259–3264, 2019, doi: 10.23919/ICPEECCEAsia42246.2019.8797022.

[23] S. Xu, Q. Qian, T. Tao, S. Lu, and W. Sun, "Small Signal Modeling and Control Loop Design of Critical Conduction Mode Active Clamp Flyback Converter", *IEEE Trans. Power Electron*, vol. 36, no. 6, pp. 7250–7263, 2011, doi: 10.1109/TPEL.2020.3040451.

[24] S. Xu *et al*, "Sampled-data modeling for PCM and ZVS controlled critical conduction mode (CrCM) active clamp Flyback (ACF) converter at variable switching frequency", *IEEE Trans. Circuits Syst. I*, pp. 1–13, 2020, doi: 10.1109/TCSI.2020.2993256.

[25] P.-H. Liu, "Small signal analysis of active clamp Flyback converters in transition mode and burst mode", *IEEEApplied Power Electronics Conference and Exposition* (APEC), Anaheim, CA, USA, pp. 241–248, 2019, doi: 10.1109/APEC.2019.8722081.

[26] Datasheet, "ATL431, ATL432 2.5-V Low Iq Adjustable Precision Shunt Regulator", TI, [*Online*] 2016, https://www.ti.com/lit/gpn/atl431.

[27] Quick Start Guide, Bode 100 Vector Network Anlyzer, OMICRON Lab, www.omicron-lab.com, 2019.

[28] "Tutorial, Multi-Output Flyback Off-Line Power Supply", onsemi, Oct 2008, https://www.onsemi.com/pub/collateral/tnd351-d.pdf.

[29] X. Huang, J. Feng, F. C. Lee, Q. Li, and Y. Yang, "Conducted EMI analysis and filter design for MHz active clamp flyback front- end converter", *IEEE Applied Power Electronics Conference and Exposition* (APEC), Long Beach, CA, USA, Mar, pp. 1534-1540, 2016, doi:10.1109/APEC.7468071.

Received 27 May 2022

Darko Vračar received the Dipl-Ing and Magister degrees in electrical engineering from the School of Electrical Engineering, University of Belgrade, Serbia in 2000 and 2007, respectively, where he is currently pursuing the PhD degree. His major field of study was power converters and drives. He is also with BRUSA Elektronik (München) GmbH, Germany. He has 21 years of industrial experience. Some areas of expertise are implementation of telecom and datacenter power supplies, and research and development of power electronics' systems, such as solar inverters, SMPS for industrial, automotive, and telecom applications. He has published several papers related to power converters and drives and holds one patent in power conversion systems. His research interests include simulation, control, and design of power converters.

Predrag V. Pejović was born in Belgrade, Serbia, in 1966. He received the Dipl-Ing and Magister degrees in electrical engineering from the University of Belgrade, Serbia, in 1990 and 1992, respectively, and the PhD degree from the University of Colorado, Boulder, USA in 1995. He rejoined the University of Belgrade in 1995, where he is currently a Professor in charge of teaching Electrical Measurements, Software Tools in Electronics, Analog Electronics, and two courses in Power Electronics. His research interests include analog circuit design, three-phase high power factor rectifiers, dynamics of nonlinear systems, electronic measurements, automated measurement systems, wireless positioning, and techniques for computer-aided analysis, design, and optimization of power electronic systems.